J. Ocean Univ. China (Oceanic and Coastal Sea Research)
DOI 10.1007/s11802-017-3286-8
ISSN 1672-5182, 2017 16 (5): 766-774
http://www.ouc.edu.cn/xbywb/
E-mail:xbywb@ouc.edu.cn

The Evolution of Water Property in the Mackenzie Bay Polynya During Antarctic Winter

XU Zhixin[1), 2), 3), 4)], GAO Guoping[3), *], XU Jianping[1), 2), 3), 4)], and SHI Maochong[1)]

1) *College of Oceanic and Atmospheric Sciences*, *Ocean University of China*, *Qingdao* 266100, *P. R. China*
2) *State Key Laboratory of Satellite Ocean Environment Dynamics (SOED)*, *State Oceanic Administration*, *Hangzhou* 310012, *P. R. China*
3) *Shanghai Ocean University*, *College of Marine Sciences*, *Shanghai* 201306, *P. R. China*
4) *The Second Institute of Oceanography*, *State Oceanic Administration*, *Hangzhou* 310012, *P. R. China*

(Received August 17, 2016; revised October 26, 2016; accepted March 5, 2017)
© Ocean University of China, Science Press and Springer-Verlag Berlin Heidelberg 2017

Abstract Temperature and salinity profile data, collected by southern elephant seals equipped with autonomous CTD-Satellite Relay Data Loggers (CTD-SRDLs) during the Antarctic wintertime in 2011 and 2012, were used to study the evolution of water property and the resultant formation of the high density water in the Mackenzie Bay polynya (MBP) in front of the Amery Ice Shelf (AIS). In late March the upper 100–200 m layer is characterized by strong halocline and inversion thermocline. The mixed layer keeps deepening up to 250 m by mid-April with potential temperature remaining nearly the surface freezing point and sea surface salinity increasing from 34.00 to 34.21. From then on until mid-May, the whole water column stays isothermally at about −1.90℃ while the surface salinity increases by a further 0.23. Hereafter the temperature increases while salinity decreases along with the increasing depth both by 0.1 order of magnitude vertically. The upper ocean heat content ranging from 120.5 to 2.9 MJ m^{-2}, heat flux with the values of 9.8–287.0 W m^{-2} loss and the sea ice growth rates of 4.3–11.7 cm d^{-1} were estimated by using simple 1-D heat and salt budget methods. The MBP exists throughout the whole Antarctic winter (March to October) due to the air-sea-ice interaction, with an average size of about 5.0×10^3 km^2. It can be speculated that the decrease of the salinity of the upper ocean may occur after October each year. The recurring sea-ice production and the associated brine rejection process increase the salinity of the water column in the MBP progressively, resulting in, eventually, the formation of a large body of high density water.

Key words Antarctic; Mackenzie Bay polynya; sea ice formation; heat flux; brine rejection

1 Introduction

The Mackenzie Bay polynya (MBP) occurs at the western and central front of the Amery Ice Shelf (AIS) in Prydz Bay (as shown in Fig.1) from late March to late October or early November (Cheng *et al*., 2012; Hou *et al*., 2011; Massom *et al*., 1998). The Prydz Bay has been regarded as the most likely candidate for the source of the Antarctic Bottom Water (AABW) (Middleton and Humphries, 1989; Nunes and Lennon, 1996; Pu *et al*., 2002; Yabuki *et al*., 2006) for its large continental embayment and the presence of the AIS as the Weddell Sea and Ross Sea regions. MBP has an average cumulative annual sea ice production of 68.2 ± 5.8 km^3 (Tamura *et al*., 2008) or 60 ± 6 km^3 (Nihashi and Ohshima, 2015), being one of the ten highest production polynyas in the Southern Ocean. The high ice production in MBP is the primary factor for the formation of the high density water which has been linked to the AABW formation as other coastal polynyas (Williams *et al*., 2008, 2010a; Ohshima *et al*., 2013; Kitade *et al*., 2014).

The formation of the high density water in MBP can affect the saline and dense shelf water from the Cape Darnley polynya (CDP) region when possibly exported westward or has an important role in the pre-conditioning of the Cape Darnley Bottom Water (CDBW) (Ohshima *et al*., 2013; Williams *et al*., 2016). There is unusually intense air-sea interaction in the polynya in other regions such as the Weddell Sea with heat fluxes in excess of 500 W m^{-2} in winter (Fahrbach *et al*., 1994). Therefore, it has significant meaning due to the unique part it plays in the air-sea interaction and in deep ocean ventilation. It is also indicative of large-scale climate changes in the polar region and has significant importance in determining the dynamics, thermodynamics and chemical characteristics of the global ocean and atmosphere (Massom *et al*., 1998).

However, due to the extreme environments in Antarctic winter and the limitation of survey ship and observing capability, it is a big challenge to conduct long time, large-scale and successive field observations. There are great limitations in both the spatial coverage and time

* Corresponding author. E-mail: gpgao@shou.edu.cn

duration of the existing observation data, especially the oceanographic observations in Antarctic winter. The lack of observations for MBP during wintertime limits our understanding of a series of physical oceanographic processes in the MBP. Therefore, taking advantage of the marine animals (*e.g.*, seals and seabirds) as autonomous ocean profilers, with temperature and salinity tags deployed on their bodies, has become an important means in surveying the high-latitude ocean, *e.g.*, the Prydz Bay region, during winter season (Costa *et al*., 2008; Williams *et al*., 2010b). To date, the research on MBP has been largely limited to its area and sea ice production by using satellite remote sensing data (Cheng *et al*., 2012; Tamura *et al*., 2008, 2016) and its contribution to CDBW (Ohshima *et al*., 2013; Williams *et al*., 2016). Here we focus on the evolution process of the water structure in the MBP by using the seal-tagged profiles data, which finally ends with the formation of the high density water.

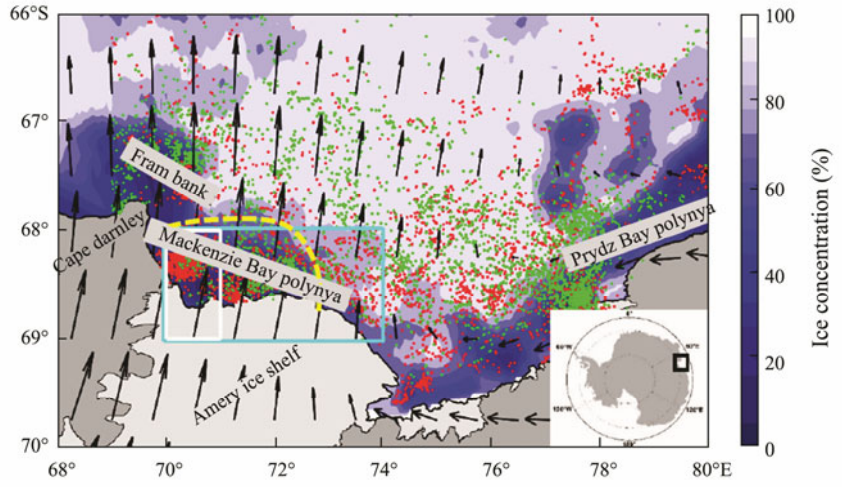

Fig.1 Geographic location of the Prydz Bay region and seal CTD profile stations in 2011 (red dots) and 2012 (green dots) within the Prydz Bay. The background is the sea ice concentration from SSMIS on March 25, 2011, overlaid by the wind field from ERA-Interim on the same day. The approximate location of the MBP is shown as a yellow dashed line. The cyan box indicates the region over which we computed the area of MBP and the CTD data in the cyan box were used to describe the seasonal variation of salinity in MBP, while the white box was chosen to discuss the thermohaline structure evolution, heat content and flux of the upper water column and sea ice growth rates. Inset shows the location of Prydz Bay in Antarctica.

In this paper, seal-tagged CTD data in the wintertime (from March to August) in 2011 and 2012, SSMIS sea-ice concentration data and ERA-Interim reanalysis dataset were used to analyze the spatial and temporal distribution of the MBP and the evolution of the thermohaline structure of the water column in Antarctic winter. The associated upper ocean heat loss and sea ice growth rates during the transition process were estimated quantitatively. The corresponding relationships among the offshore wind, air temperature, polynya extent, sea surface net heat flux and upper ocean salinity were discussed to reveal the formation, variation and persistence of the MBP impacted by the atmosphere-sea ice-ocean coupling interactions. The vital role the MBP plays on the high density water formation in the Prydz Bay was also investigated.

2 Data and Methods

2.1 Seal-Tagged CTD Data

CTD data used in this paper were obtained by the autonomous CTD-Satellite Relay Data Loggers (CTD-SRDLs) deployed on the heads of the southern elephant seals in the Australian Integrated Marine Observing Systems (IMOS). Seals dove repeatedly to retrieve data profiles, and sent back 3.5 vertical profiles per day on average via the Argos satellite system when they surfaced. Fig.1 shows the geographic location of the Prydz Bay region and the CTD profile stations.

Most of the maximum depth of CTD-SRDLs profile data collected are confined to 500 m, while only a few can reach 800 m, or 1000 m, which are mainly distributed in the shelf break area and the slope basin outside the Prydz Bay. The accuracies of CTD-SRDLs hydrographic measurements are about 0.03℃ in temperature and 0.05 or better in salinity after being post-processed using a set of delay-mode techniques (Roquet *et al*., 2011). It should be pointed out that although there are about 8400 CTD profiles in the Prydz Bay and its adjacent sea area during austral winter in 2011 and 2012, less than 400 profiles are located within the study area, among which there are about 280 profiles in 2011 from March 24 to June 21 and 115 profiles in 2012 from March 27 to August 7.

2.2 Environmental Data

Daily remote-sensing sea-ice concentration data from January 1, 2011 to December 31, 2012, retrieved from the 91 GHz channels of the Special Sensor Microwave Imager/Sounder (SSMIS), were obtained from the Institute of Environmental Physics, University Bremen, with 6.25 km spatial resolution, and the website is http://www.iup. uni-bremen.de:8084/ssmis/. As for the atmospheric data, we use the ERA-Interim reanalysis data at a grid cell of

0.75°×0.75° from the European Center for Medium-Range Weather Forecasts (ECMWF) in the same periods, which include the 2 meter air temperature, wind speed, surface heat flux, *etc*. The air temperature and wind data are available four times a day, so we averaged them to obtain the daily values. For the surface heat flux data, published at 0:00 and 12:00 every day with step of twelve, we summed them up as the daily values.

2.3 Estimations of Heat Content, Flux and Sea Ice Growth Rate

Due to the inhomogeneity of the spatial and temporal distribution of the seal data, the ocean heat content, heat flux and sea-ice growth rate were estimated within a small square region between 68°–69°S, 70°–74°E (white box, Fig.1) where there are concentrated profile data without remarkable spatial variation, in order to reduce the resulting error and ensure the reliability of the estimates.

Following Costa *et al*. (2008), we estimated the upper ocean heat content (Q, J m^{-2}) as follows:

$$Q = \int_{Z_2}^{Z_1} \rho_0 c_p (T_z - T_f) \mathrm{d}z ,$$

where ρ_0 is the density of seawater (1027 kg m^{-3}); c_p is the specific heat of seawater (3994.6 J ℃$^{-1}$ kg^{-1}); T_z is the measured temperature value; and T_f = −1.89℃ is the surface freezing point, which was calculated at an average salinity of 34.37 and a pressure of 0 dbar using the method in Millero (1978). Q was obtained by integrating the heat content over a range of depth from the surface (Z_1) to 200 m (Z_2). The ocean heat flux (Q_F, W m^{-2}) was estimated as the temporal change of the integrated heat content:

$$Q_F = \frac{\mathrm{d}Q}{\mathrm{d}t} .$$

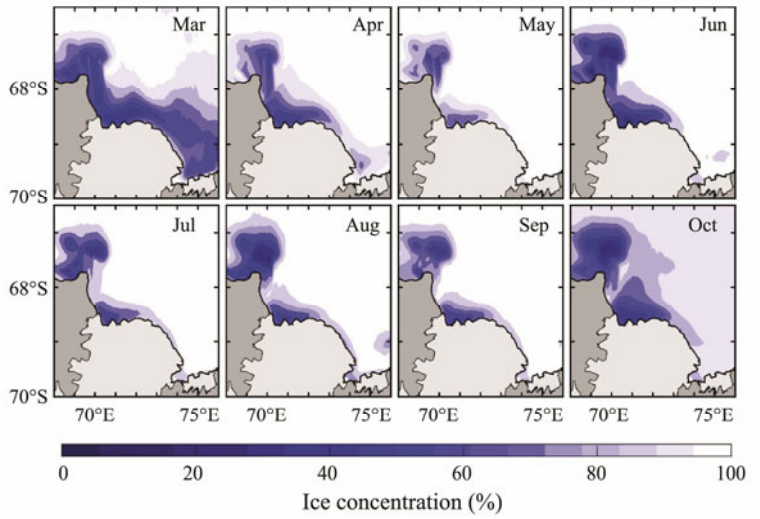

Fig.2 Monthly mean sea-ice concentration distribution in front of the AIS in 2011.

We estimated sea ice production using the 1-D salinity budget method detailed in Charrassin *et al*. (2008).

$$\rho_0 V_0 S_0 = \rho_0 V_f S_f + \rho_i V_i S_i ,$$

where ρ_0 is the sea water density, as above; V_0 is the initial volume of water, with initial salinity S_0; V_i is the volume of ice formed with density ρ_i = 920 kg m^{-3} and salinity S_i = 10; and V_f= V_0 − V_i is the final volume of the seawater with salinity S_f. The calculation of ice formation assumed no contribution from horizontal advection and is based on the salinity of the upper 200 m considering the depth range of the observation data.

Estimates of the surface net heat flux (Q_{SF}) were performed using the following equation:

$$Q_{SF} = Q_S + Q_L + Q_H + Q_E ,$$

where Q_S is the shortwave radiation flux; Q_L is the net longwave radiation flux; Q_H and Q_E are the sensible and latent heat fluxes, respectively. The four heat flux components were reanalysis data production directly provided by the ECMWF.

3 Properties and Variations of MBP

3.1 Spatial and Temporal Distribution

The sequences of daily ice concentration images over the study area (not shown) during winters (March to October) of 2011–2012 show the basic characteristics of the MBP in terms of persistence, size, location and shape. MBP occurs on March 9 and lasts until November 22 in 2011 while existing during the period from March 25 to December 25 in 2012, which proves to emerge later than that in 2011 as well as the disappearing timing. The MBP areal extent will change correspondingly with the atmosphere-sea ice-ocean coupling interaction. Transient polynya closure arises occasionally during the occurrence period; the results of calculation of the daily MBP areal extent show that the durations of the occurrence of MBP in 2011 and 2012 are 259 days and 243 days, respectively. Monthly

mean sea-ice concentration distribution in front of the AIS in 2011 is shown in Fig.2, from which we can see MBP almost persists for the entire winter from March to October. The center of the polynya is fixed at the middle west front of the AIS and its spatial shape is consistent with the trend of AIS with its southern edge adjoining to the front edge of the AIS. The MBP possesses typical features of the coastal polynya induced by the offshore wind. A line of small grounded icebergs extends northeast from Cape Darnley, leading to extensive and frequent fast ice coverage between 68°–71°E, and this fast ice frequently extends to the western edge of the Amery Ice Shelf, while between 71°–74°E, there is no fast ice (Fraser *et al*., 2012; Nihashi and Ohshima, 2015). In March 2011, MBP is joined with the west CDP and the east Prydz Bay Polynya (PBP), forming a whole area in front of the AIS covered by thin ice, with a north-south width of about 50 km. In April, the scope of sea ice cover expands and MBP narrows significantly compared to that in March because of the continuous atmospheric cooling effect. From May to September, MBP is encompassed by fast ice and floating pack ice with no obvious change in size and located primarily between 70°–73°E at the western and central fronts of the AIS. In October, the concentration of the ice-bound area in Prydz Bay is between 80%–90%, which is lower than those in the other months. The variation trend of MBP is in accordance with that in Cheng *et al*. (2012) as a whole.

The spatial and temporal variation in the winter of 2012 is roughly consistent with that in 2011 (not shown). It occurs in the late March, a little later than in last year. In June, the MBP size is much smaller while sea ice concentration in MBP is much higher than those in the same month of 2011. From July to October, MBP prince-pally emerges at the middle west front of the AIS, with sea ice concentration of the central region to be 10%–40%.

On the whole, according to the sea ice concentration distribution from satellite remote sensing in the winters of 2011 and 2012, the center of MBP is mainly located between 70°–72°E and it can border the CDP to the west in March while separated from CDP by the fast ice on the Fram Bank in other months. It can spread eastward to approximately 74°E, be connected with the PBP and extend to the north of about 68°S, generally not exceeding the Cape Darnley.

3.2 Thermohaline Structure and Its Variation in MBP

3.2.1 Vertical distribution

Fig.3 illustrates the vertical distributions of all the CTD profiles in the study area. It presents the evolution process of the upper water column within MBP from the remnant summer stratification to the new winter vertically homogenous state.

In late March, when the Antarctic enters into winter, the surface layer water starts to get cold due to the atmospheric cooling effect. The greatest thermohaline variation is observed in the layer from the surface to 100–200 m depth, characterized by strong halocline and inversion thermocline. Below this upper layer, the water column is nearly isothermal and the vertical stability is preserved by

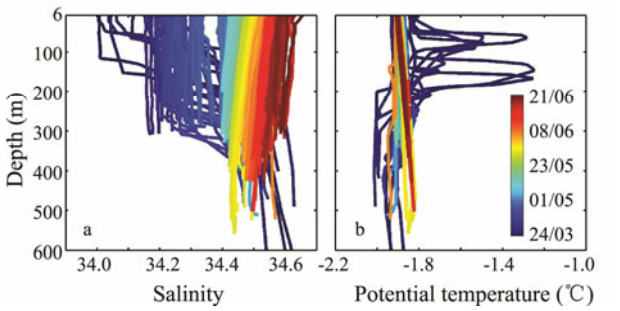

Fig.3 Vertical profiles of (a) salinity and (b) potential temperature from seal CTD data in 2011. The color scale on panel b is the date.

the slightly increasing salinity. As the air temperature continues to decrease and the vertical convection strengthens in response to the brine rejection by sea-ice formation, the mixed layer keeps deepening to 250 m by mid-April and the potential temperature decreases from −1.28℃ at 64 m depth to nearly the surface freezing point throughout the upper 400 m simultaneously, indicating the complete disappearance of the sub-surface warm water. Correspondingly, the sea surface salinity increases from 34.00 to 34.21. From then on until mid-May, the whole water column stays isothermally at about −1.90℃ while the surface salinity increases by a further 0.23. Hereafter the temperature increases while salinity decreases along with the depth by 0.1 order of magnitude vertically, resulting in the upper potential density slightly greater than the lower layer. This structural instability contributes to the transporttation of surface cold and salty water to the ocean interior.

Although in the winter of 2012, there are fewer CTD profiles in the study area than those in 2011, the evolution processes of the potential temperature and salinity along with time and depth (Figures not shown) are still very clear and have no great difference with those in 2011.

3.2.2 *θ*–*S* characteristic

Potential temperature (θ, ℃) and salinity (S) data obtained in the study area were extracted to construct the θ–S diagram as shown in Fig.4. There are generally two distribution shapes in the diagram. One is the ‘dome’ shape, and the other is a straight-line shape distributed along the surface freezing line. Based on the previous research (Xu *et al*., 2016, 2018), there are mainly four water masses in the study area, Antarctic Surface Water (AASW), Prydz Bay Subsurface Water (PBSSW), Prydz Bay Shelf Water (SW) and Prydz Bay Ice Shelf Water (ISW). Among them, High Salinity Shelf Water (HSSW) and High Salinity Ice Shelf Water (HSISW) are the most distinctive ones. Under the coaction of the atmospheric cooling effect and the sea ice formation and brine rejection process, the upper water column within MBP becomes colder and saltier

progressively over time, generating intensified convective mixing, so that PBSSW quickly disappears and θ–S distribution shape also under-goes the transition from the 'dome' shape to straight-line shape. AASW is primarily observed at the upper layer, with potential temperature between −1.90℃ and −1.00℃ and salinity between 33.96–34.40. Below this layer the water column is occupied by the High Salinity Shelf Water (HSSW) with potential temperature below −1.80℃ and salinity over 34.40. It must be pointed out that ISW is detected at intermediate depths (250–450 m), characterized by potential temperature colder than the surface freezing point (−1.90℃) and salinity ranging from 34.17 to 34.66. ISW is supposed to be produced by the interaction between HSSW and the AIS (Carmack and Foster, 1975), *i.e.*, the deep layer of the MBP area is principally occupied by HSSW and HSISW in austral winter.

θ–S diagram for the profiles in the study area in 2012 presents the 'dome' shape and straight-line shape as well (not shown), but the straight-line shape seems like much shorter, not as significant as that in 2011. Salinity is generally higher than 34.40 while potential temperature remains at nearly the freezing point, which demonstrates that the characteristic of low temperature and high salinity of water at lower depth is more conspicuous. This difference is mainly related to the difference of observation time of the two years. In 2011 the last profile was observed on June 21 while in 2012 the last one observed on August 7. When entering into the late winter, the cold and salty water within MBP becomes more vertically homogeneous and the salinity is also higher than that in the early winter.

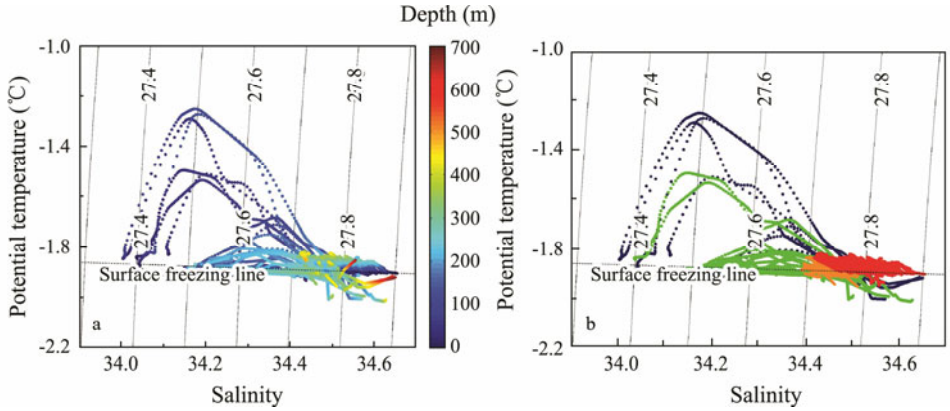

Fig.4 θ–S scatter diagram of the CTD profiles collected in the study area in 2011. (a) The color represents depth. (b) Blue represents March, green represents April, orange represents May, and red represents June.

3.2.3 Seasonal variability of salinity

Fig.5 shows the vertical and temporal variations of salinity obtained for profiles in the MBP (cyan box in Fig.1) at the depths of 6 m, 100 m, 200 m and 500 m.

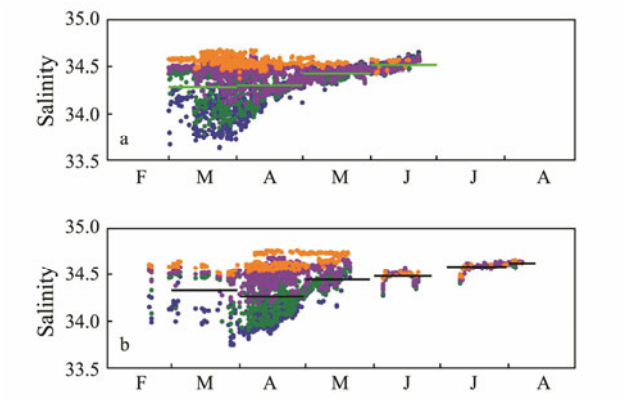

Fig.5 Vertical and temporal variations of salinity in MBP from February to August in (a) 2011 and (b) 2012, at depths of 6 m (blue), 100 m (green), 200 m (purple) and 500 m (orange), and the horizontal lines represent the monthly mean salinities averaged over the 6–200 m depth range.

In February and March, significant variations of salinity are observed at the upper 200 m layer, exhibiting obvious trend of salinity increasing with depth. After mid-April, the salinity becomes vertically homogeneous gradually and salinities below 200 m depth basically remain constant over time. The mean salinities over 6–200 m of each month from March to August are displayed as the horizontal lines in Fig.5a–b, which clearly presents seasonal evolution and demonstrates that the salt-released process by sea-ice formation within MBP in winter can continuously increase the salinity of the water column.

3.3 Upper Ocean Heat Content, Heat Flux and Sea Ice Growth Rate in MBP

The significant water-mass modification is accompanied by high salt flux into the ocean associated with notable ice growth and great heat loss to the atmosphere. Thus, the upper ocean heat content and flux averaged over the 200 m depth range and sea-ice growth rates in each period were estimated, as shown in Table 1. Both the ocean heat content and flux can be expected to decrease and asymptotically approach zero as the temperature of the water column turns to nearly the freezing point when given the absence of any lateral advection of heat into the region. The upper ocean heat content peaks at 120.5 MJ m^{-2} in March, then dramatically decreases to 25.6 MJ m^{-2} in April and thereafter keeps the decreasing trend during May and June with values of 2.9–6.1 MJ m^{-2}. From June to August

in 2012, the upper ocean heat content (32.0–34.0 MJ m^{-2}) seems to be slightly higher, but still much lower than that in March 2011, which has a close relationship with the shift of air temperature and polynya areal extent. The oceanic heat loss to the atmosphere is at least an order of magnitude greater than that for an ice-covered ocean (Gordon, 1982). Therefore, it is very likely that the upper ocean heat content will decrease with the continuously decreasing air temperature and shrinking polynya size during the winter season. This can also be corroborated by the variation trend of the upper ocean heat flux, which fell to −28.4 W m^{-2} in June from as high as −187.5 W m^{-2} in March 2011 and ranged from −17.0 W m^{-2} (in June) to −9.8 W m^{-2} (in August) in 2012. The results seem to be much lower than the average heat flux (−430 W m^{-2}) from the CDP estimated from a high-temporal-resolution study by Potter (1995). But the fact reflected by these changes is supposed to be consistent. When the winter comes, the high upper ocean heat content dropped sharply with the decreasing temperature, causing the ocean to release more heat to the atmosphere. As entering into the deep winter, heat loss from the ocean to the atmosphere continually reduced with the decrease of the upper ocean heat content.

Table 1 The statistical results of ocean heat content, heat flux and sea-ice formation rates in MBP

Periods for averaging	No. of profiles	6–200 m ocean heat content (MJ m^{-2})	6–200 m ocean heat flux (W m^{-2})	Sea-ice formation rate (cm d^{-1})
March 24–31, 2011	4	120.5	−287.0	11.7
April 1–30, 2011	57	25.6	−91.4	9.3
May 1–31, 2011	93	2.9	−50.0	6.6
June 1–21, 2011	117	6.1	−28.4	7.1
June 6–16, 2012	36	34.0	−17.0	6.6
July 12–31, 2012	60	33.9	−15.7	5.8
August 1–7, 2012	14	32.0	−9.8	4.3

Seal measurements of changes in salinity below the sea ice provide a unique dataset, enabling the sea-ice growth rates to be estimated by using the simple 1-D salinity budget for the upper 200 m of the water column (Charrassin *et al*., 2008). This method assumes no contribution from horizontal advection to salinity variability, which cannot be assessed from the seal data. As can be seen from Table 1, in the early winter (March), when the upper oceanic heat loss peaks, sea ice formation rate also attains the maximum value of 11.7 cm d^{-1}. From April to August, sea ice formation rate overall exhibits a downward trend with values between 9.3–4.3 cm d^{-1}, albeit some slight fluctuations. Marsland *et al*. (2004) stated that sea ice formed over the Adelie Depression at a rate of 4.9 cm d^{-1} in wintertime (May to September) for the period 1991–2000 based on a variant of the Max Planck Institute Ocean Model (MPIOM). Moreover, an ice formation rate in the range of 0.8–3.0 cm d^{-1} from April to August 2004 at four different positions located in the Indian Ocean sector near the Antarctic continent was revealed by elephant seals measurements (Charrassin *et al*., 2008). Compared with these previous studies, our estimates seem a little bit higher. The biases are supposed to be ascribed to the difference of the study area and methods from the previous studies above. On the other hand, the results basically do have good agreement in magnitude. Moreover, our estimates are of the same order of magnitude as the satellite derived sea ice formation rates in the MBP with the annual mean values of 22 years (Tamura *et al*., 2016), there being a difference of 30%. Further comparative analysis indicates that during the transition from early winter to late winter, along with the gradual reduction of the upper ocean heat released into the atmosphere, sea ice formation rate also decreases. But even until August, both the two processes have not ceased, which indirectly suggests the existing of MBP throughout the whole winter. The salinity of the water column constantly increases while the ocean loses its heat successively within polynya (Gao *et al*., 2016), which is the unique characteristic of the polynya. Continual sea ice formation leads to the increase of the surface layer salinity, then it will momently destroy the stability of the water and strengthen the vertical convection, and eventually result in the increasing of the bottom layer salinity.

4 Discussion and Conclusions

4.1 Katabatic Wind and MBP Areal Extent

In order to further understand the unique characteristic of the MBP, the monthly mean MBP areal extent bounded by the cyan box in Fig.1 was calculated during the simultaneous occurrence period of MBP in 2011 and 2012 (March 25 to October 13), based upon the spatial and temporal variability of MBP discussed in the preceding sections. In previous studies, coastal polynyas were detected by utilizing thin ice thickness (<0.2 m) algorithm, which takes advantage of 85-GHz and 37-GHz brightness temperature data retrieved from Special Sensor Microwave Imager (SSM/I) (Martin *et al*., 2007; Nihashi and Ohshima, 2015; Tamura *et al*., 2007, 2008, 2016) or a two-dimensional polynya signature simulation method (PSSM) with passive microwave data (Markus and Burns, 1995). In this paper, the 75% ice-concentration threshold (Massom *et al*., 1998) was chosen for simplicity. Although it was not the best one and might have relatively large ambiguity, it was enough to meet the need of our research.

First of all, the relationship between katabatic wind and MBP areal extent was discussed in this part. There are five grid points of the ERA-Interim dataset exactly located in the research area. Considering the geographic position and topographic characteristic of the AIS, southwest 45 degrees was chosen as the major direction

of the offshore wind, along which we calculated the magnitude of this component of the wind vector, and then averaged out the five points. Figs.6a–b shows the time series of the offshore component of katabatic wind and the MBP areal extent for the years 2011 and 2012. Both of them vary greatly every day and fluctuate on roughly synoptic timescales based on an 8-day running mean. MBP areal extent ranges from 0.03×10^4 km^2 to 1.54×10^4 km^2. In 2011, the maximum and minimum values are 0.65×10^4 km^2 and 0.24×10^4 km^2, appearing in March and May respectively. In 2012, the extrema are 0.76×10^4 km^2 (in March) and 0.23×10^4 km^2 (in June), respectively. The estimated mean MBP areal extents of 2011 and 2012 are 0.53×10^4 km^2 and 0.46×10^4 km^2, which are a little higher than the annual average of 0.35×10^4 km^2 for years 1987–1994 (Massom *et al*., 1998) and close to the mean thin ice area of $(0.51\pm0.06)\times10^4$ km^2 during winters (March–October) from 1992 to 2013 (Tamura *et al*., 2016).

The time series in Fig.6 also manifest that both the offshore wind and MBP areal extent have great daily fluctuation without conspicuous change cycle, and present variations on roughly synoptic timescales after applying an 8-day running mean to smooth the high frequency perturbations. Intermittent polynya closure, occurring on some days, is largely attributed to a sharp decrease in wind speed or a reversal in wind direction, which results in quickly freezing of the open water. Strong winds act to break up the ice cover, remove the ice and facilitate the formation or expansion of open water. Specific correlation coefficients of the monthly mean values of the two variables for each month were computed. They are generally around 0.65 with the maximum value to be 0.97, demonstrating that there is a good correlation between them in austral winter. The values of coefficient also have good agreement with the result (0.64) of Nihashi and Ohshima (2015).

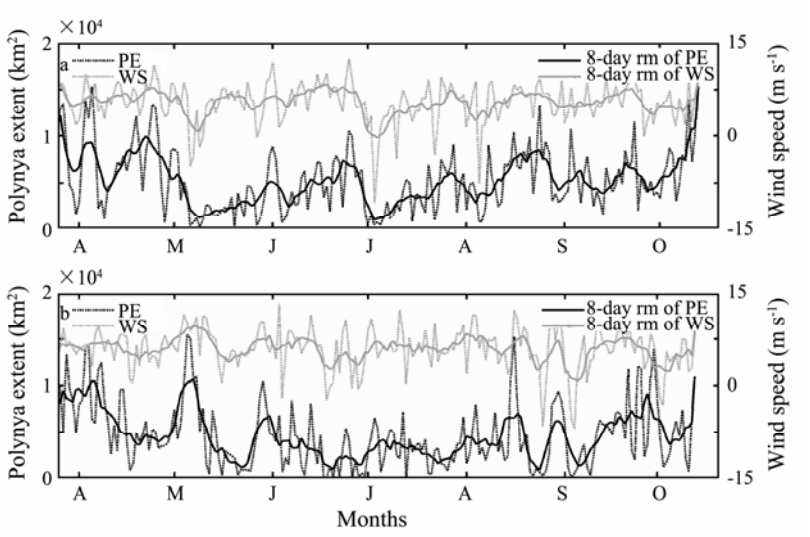

Fig.6 Daily time series of the MBP areal extent (black dashed line) and the offshore component of katabatic wind (gray dashed line) in (a) 2011 and (b) 2012. 8-day running means (rm) of the two variables are also shown (black solid line and gray solid line, respectively).

4.2 Relationship Between Areal Extent, Air Temperature and Net Surface Heat Flux

In addition to the wind forcing effect, MBP areal extent is also affected by air temperature and net surface heat flux. Fig.7 shows the time series of monthly mean MBP areal extent, net heat flux at sea surface, 2 meter air temperature and salinity averaged over the 6–200 m depth range in 2011 and 2012. It is not hard to find that there is one-to-one correspondence among the distributions of MBP areal extent, air temperature and net surface heat flux. Specifically, corresponding to lower air temperature and greater oceanic heat loss to the atmosphere is the smaller MBP areal extent, and vice versa.

Fig.7 also manifests that when Prydz Bay enters into winter and the temperature is continually falling, the direction of the net surface heat flux changes from downward (before January) to upward (after February) and MBP areal extent shrinks, indicating the continuously strengthening of the sea ice formation and brine rejection process. At the same time the salinity of the water column constantly increases. Despite the lack of salinity data after August, it can be speculated that the decrease of the salinity of the upper ocean may occur after October each year according to the slow variation of the MBP areal extent, air temperature and sea surface net heat flux from May or June to August or September. That is, during most of the winter time, the average salinity of the water column within MBP remains above 34.40 or higher.

5 Conclusions

Seal-tagged CTD observations collected over the wintertime (from March to August) 2011–2012 have allowed us to evaluate the evolution of water property in the MBP and its important contribution to the formation of the high density water in the Prydz Bay.

MBP emerges at the middle west front of the AIS in aus-

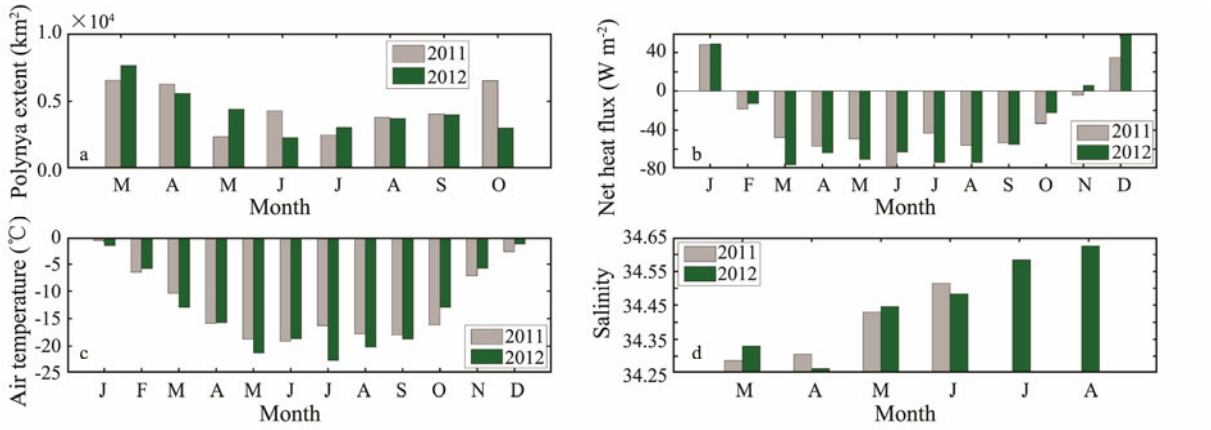

Fig.7 Monthly mean of (a) MBP areal extent, (b) net heat flux at sea surface, (c) 2 meter air temperature and (d) salinity averaged over 6–200 m depth range in 2011 (gray) and 2012 (green).

tral winter, and its center is located between 70°–72°E. It can border the CDP to the west and spread eastward to approximately 74°E and connect with the PBP. To the north it extends to about 68°S, generally not exceeding the Cape Darnley.

Thermohaline structure within MBP transforms from the remnant late-summer stratification to the new winter vertically homogenous state. AASW with low temperature (−1.90℃ to −1.00℃) and low salinity (33.96 – 34.40) is primarily observed at the upper 200 m layer and the deep below is mainly occupied by the High Salinity Shelf Water (HSSW) (<−1.80℃, >34.40) and High Salinity Ice Shelf Water (HSISW) (<−1.89℃, >34.50).

The upper ocean heat content within MBP ranges from 120.5 to 2.9 MJ m^{-2}, while heat flux has the values of 9.8–287.0 W m^{-2} loss and sea ice growth rates are of 4.3–11.7 cm d^{-2}. The maximum average sea ice growth rate occurs in the period from March to April each year.

The MBP areal extent is closely related to the offshore wind and has good correspondence with net surface heat flux and 2 meter air temperature. When the offshore wind is weak, the temperature is low, and the oceanic heat loss is great, the MBP size will be small, and vice versa.

The sea ice formation and brine rejection process almost lasts the whole winter, leading to the continuously increasing of the salinity. The decrease of the salinity of the upper ocean may occur after October each year. During most of the winter time, the average salinity of the water column within MBP remains above 34.40 or higher.

So the atmosphere-sea ice-ocean coupling interaction, including the AIS, the strong offshore wind, cold air temperature, rapid sea-ice growth rate and the great oceanic heat loss to the atmosphere, leads to the persistent existence of the MBP during the whole wintertime. Moreover, the recurring sea-ice production and the associated brine rejection process increases the salinity of the water column in the MBP progressively. The increase of the density of the upper ocean will destroy the stability of the water, strengthen the vertical convection, and result in the continual increasing of the density of the deep water below, along with the ocean constantly releasing heat to the atmosphere during this process. All of the above constitute the necessary prerequisite for the likely formation of the AABW in Prydz Bay.

As for whether the high density water formed in the MBP will move northward through the Amery Depression into the shelf break region, then sink down the slope and mix with CDW, and finally flow into AABW, it requires to be verified by flow field observations or simulated computation. This will be explored in more detail in the next article.

Acknowledgements

This research is supported by the Science and Technology Basic Work of the Ministry of Science and Technology of China (No. 2012FY112300) It is our pleasure to thank Prof. Mark Hindell from the University of Tasmania, Australia, for providing the IMOS Seal-CTD data.

References

Carmack, E. C., and Foster, T. D., 1975. On the flow of water out of the Weddell Sea. *Deep Sea Research and Oceanographic Abstracts*, **22** (11): 711-724.

Charrassin, J. B., Hindell, M., Rintoul, S. R., Roquet, F., Sokolov, S., Biuw, M., Costa, D., Boehme, L., Lovell, P., Coleman, R., Timmermann, R., Meijers, A., Meredith, M., Park, Y. H., Bailleul, F., Goebell, M., Tremblay, Y., Bost, C. A., McMahon, C. R., Field, I. C., Fedak, M. A., and Guinet, C., 2008. Southern ocean frontal structure and sea-ice formation rates revealed by elephant seals. *Proceedings of the National Academy of Sciences of the United States of America*, **105** (33): 11634-11639.

Cheng, Y. Y., Shi, J. X., and Zheng, S. J., 2012. Temporal and spatial variation of the Mackenzie Bay Polynya, Antarctica and its main impact factors. *Periodical of Ocean University of China*, **42**: 1-9 (in Chinese with English abstract).

Costa, D. P., Klinck, J. M., Hofmann, E. E., Dinniman, M. S., and Burns, J. M., 2008. Upper ocean variability in west Antarctic Peninsula continental shelf waters as measured using instrumented seals. *Deep Sea Research Part II Topical Studies in Oceanography*, **55** (3-4): 323-337.

Fahrbach, E., Augstein, E., and Olbers, D., 1994. Impact of shelf

and sea ice on water mass modifications and large-Scale oceanic circulation in the Weddell Sea. In: *Antarctic Science*. Hempel, G., ed., Springer, Heidelberg, Berlin, 167-187.

Fraser, A. D., Massom, R. A., Michael, K. J., Galtonfenzi, B. K., and Lieser, J. L., 2012. East Antarctic landfast sea ice distribution and variability, 2000–08. *Journal of Climate*, **25** (4): 1137-1156.

Gao, G. P., Yan, M. F., Xu, Z. X., and Cheng, L. Q., 2016. The evolution of upper water structure in the Prydz Bay polynya region during Antarctic winter, 2011. *Chinese Journal of Polar Research*, **28** (2): 219-227 (in Chinese with English abstract).

Gordon, A. L., 1982. Weddell deep water variability. *Journal of Marine Research*, **40**: 199-217.

Hou, J., Shi, J., Heygster, G., and Cheng, Y., 2011. Area of a polynya at Amery Ice Shelf derived from AMSR-E 89 GHz sea ice concentrations and MODIS images. *Proceedings of the International Conference on Remote Sensing, Environment and Transportation Engineering*, Nanjing, 124-127.

Kitade, Y., Shimada, K., Tamura, T., Williams, G. D., Aoki, S., Fukamachi, Y., Roquet, F., Hindell, M., Ushio, S., and Ohshima, K. I., 2014. Antarctic bottom water production from the Vincennes Bay polynya, East Antarctica. *Geophysical Research Letters*, **41** (10): 3528-3534.

Markus, T., and Burns, B. A., 1995. A method to estimate subpixel-scale coastal polynyas with satellite passive microwave data. *Journal of Geophysical Research Oceans*, **100** (C3): 4473-4487.

Marsland, S. J., Bindoff, N. L., Williams, G. D., and Budd, W. F., 2004. Modeling water mass formation in the Mertz glacier polynya and Adélie Depression, East Antarctica. *Journal of Geophysical Research*, **109** (C11): 640-645.

Martin, S., Drucker, R. S., and Kwok, R., 2007. The areas and ice production of the western and central Ross Sea polynyas, 1992–2002, and their relation to the B-15 and C-19 iceberg events of 2000 and 2002. *Journal of Marine Systems*, **68** (1): 201-214.

Massom, R. A., Harris, P. T., Michael, K. J., and Potter, M. J., 1998. The distribution and formative processes of latent-heat polynyas in East Antarctica. *Annals of Glaciology*, **27**: 420-426.

Middleton, J. H., and Humphries, S. E., 1989. Thermohaline structure and mixing in the region of Prydz Bay, Antarctica. *Deep Sea Research Part A. Oceanographic Research Papers*, **36** (8): 1255-1266.

Millero, F. J., 1978. Freezing point of sea water. Eighth Report of the Joint Panel of Oceanographic Tables and Standards, appendix. *Unesco Technical Paper in Marine Science*, **28**: 29-31.

Nihashi, S., and Ohshima, K. I., 2015. Circumpolar mapping of Antarctic coastal polynyas and landfast sea ice: Relationship and variability. *Journal of Climate*, **28** (9): 3650-3670.

Nunes, V. R. A., and Lennon, G. W., 1996. Physical oceanography of the Prydz Bay region of Antarctic waters. *Deep Sea Research Part I: Oceanographic Research Papers*, **43** (5): 603-641.

Ohshima, K. I., Fukamachi, Y., Williams, G. D., Nihashi, S., Roquet, F., Kitade, Y., Tamura, T., Hirano, D., Borreguero, H. L., Field, L., Hindell, M., Aoki, S., and Wakatsuchi, M., 2013. Antarctic bottom water production by intense sea-ice formation in the Cape Darnley polynya. *Nature Geoscience*, **6** (3): 235-240.

Potter, M. J., 1995. An evaluation of polynyas in East Antarctica. Bachelor thesis. University of Tasmania.

Pu, S. Z., Hu, X. M., Dong, Z. Q., Yu, F., and Chen X. R., 2002. Features of circumpolar deep water, Antarctic bottom water and their movement near the Prydz Bay. *Acta Oceanologica Sinica*, **24** (3): 1-8 (in Chinese with English abstract).

Roquet, F., Charrassin, J. B., Marchand, S., Boehme, L., Fedak, M., Reverdin, G., and Guinet, C., 2011. Delayed-mode calibration of hydrographic data obtained from animal-borne satellite relay data loggers. *Journal of Atmospheric & Oceanic Technology*, **28** (6): 787-801.

Tamura, T., Ohshima, K. I., and Nihashi, S., 2008. Mapping of sea ice production for Antarctic coastal polynyas. *Geophysical Research Letters*, **35** (7): 284-298.

Tamura, T., Ohshima, K. I., Fraser, A. D., and Williams, G. D., 2016. Sea ice production variability in Antarctic coastal polynyas. *Journal of Geophysical Research*, **121**: 2967-2979.

Tamura, T., Ohshima, K. I., Markus, T., Cavalieri, D. J., Nihashi, S., and Hirasawa, N., 2007. Estimation of thin ice thickness and detection of fast ice from SSM/I data in the Antarctic Ocean. *Journal of Atmospheric & Oceanic Technology*, **24** (10): 431-443.

Williams, G. D., Aoki, S., Jacobs, S. S., Rintoul, S. R., Tamura, T., and Bindoff, N. L., 2010a. Antarctic bottom water from the Adélie and George V Land coast, East Antarctica (140–149°E). *Journal of Geophysical Research: Oceans*, **115** (C4): C04027.

Williams, G. D., Bindoff, N. L., Marsland, S. J., and Rintoul, S. R., 2008. Formation and export of dense shelf water from the Adélie Depression, East Antarctica. *Journal of Geophysical Research: Oceans*, **113** (C4): C04039.

Williams, G. D., Herraiz-Borreguero, L., Roquet, F., Tamura, T., Ohshima, K. I., Fukamachi, Y., Fraser, A. D., Gao, L., Chen, H., McMahon, C. R., Harcourt, R., and Hindell, M., 2016. The suppression of Antarctic bottom water formation by melting ice shelves in Prydz Bay. *Nature Communincations*, **7**: 12577, DOI: 10.1038/ncomms12577.

Williams, G. D., Hindell, M., Houssais, M. N., and Tamura, T., 2010b. Upper ocean stratification and sea ice growth rates during the summer-fall transition, as revealed by elephant seal foraging in the Adélie Depression, East Antarctica. *Ocean Science*, **7** (2): 185-202.

Xu, Z. X., Gao, G. P., Xu, J. P., and Cheng L. Q., 2018. Distribution of water masses and high density water near the Amery Ice Shelf in Antarctic winter, 2012. *Chinese Journal of Polar Research* (Accepted) (in Chinese with English abstract).

Xu, Z. X., Xu, J. P., Gao, G. P., and Shi, M. C., 2016a. Study on hydrographic features and water masses in the Prydz Bay and its adjacent waters in Antarctic winter of 2011. *Advances in Marine Science*, **34** (2): 226-239 (in Chinese with English abstract).

Yabuki, T., Suga, T., Hanawa, K., Matsuoka, K., Kiwada, H., and Watanabe, T., 2006. Possible source of the Antarctic bottom water in the Prydz Bay region. *Journal of Oceanography*, **62** (5): 649-655.

(Edited by Chen Wenwen)